Size distribution of submarine landslides and its implication to tsunami hazard in Puerto Rico

Uri S. ten Brink,[1] Eric L. Geist,[2] and Brian D. Andrews[1]

Received 23 February 2006; revised 27 April 2006; accepted 4 May 2006; published 13 June 2006.

[1] We have established for the first time a size frequency distribution for carbonate submarine slope failures. Using detailed bathymetry along the northern edge of the carbonate platform north of Puerto Rico, we show that the cumulative distribution of slope failure volumes follows a power-law distribution. The power-law exponent of this distribution is similar to those for rock falls on land, commensurate with their interpreted failure mode. The carbonate volume distribution and its associated volume-area relationship are significantly different from those for clay-rich debris lobes in the Storegga slide, Norway. Coupling this relationship with tsunami simulations allows an estimate of the maximum tsunami runup and the maximum number of potentially damaging tsunamis from landslides to the north shore of Puerto Rico. **Citation:** ten Brink, U. S., E. L. Geist, and B. D. Andrews (2006), Size distribution of submarine landslides and its implication to tsunami hazard in Puerto Rico, *Geophys. Res. Lett.*, *33*, L11307, doi:10.1029/2006GL026125.

1. Introduction

[2] The mitigation of earthquake hazard via the modification of building codes is based on probabilistic estimates of ground shaking within a given time period [*Cornell*, 1968]. These estimates are based, among other things, on the fact that the frequency of earthquakes as a function of earthquake magnitude follows a power-law distribution. This distribution allows us to estimate the number of earthquakes from incomplete observations and is indicative of the fundamental processes behind the generation of earthquakes [e.g., *Rundle et al.*, 2003]. It has been suggested that the area and volume of subaerial landslides also follow a power-law distribution [*Fuyii*, 1969; *Sugai et al.*, 1994; *Dussauge et al.*, 2003; *Malamud et al.*, 2004]. To date only one submarine slope failure distribution was established [*Issler et al.*, 2005], but interest in submarine landslides is increasing because they are known to have generated destructive tsunamis [*Piper et al.*, 1999; *Satake and Tanioka*, 2003; *Ward*, 2001].

[3] The north shore of Puerto Rico and its offshore region are covered by thick layers of carbonate rocks that now dip northward at an angle of 4° (Figure 1). These layers were deposited horizontally near sea level, and were titled about 3.3 Ma, such that their northernmost extent is at a depth of 4000 m and their southern extent on land in Puerto Rico is at a reconstructed elevation (before erosion) of +1300 m [*ten Brink*, 2005]. The tilt episode may have been very short, $\leq$40 kyr [*ten Brink*, 2005]. The tilting has likely increased the probability of seismically induced landslides. Tectonic motions, such as the opening of Mona rift and the subduction of the North American plate, continue to shape the area and generate earthquakes that can trigger landslides. In fact, two devastating tsunamis, associated with moderately large earthquakes, have struck the region north of Puerto Rico and the Dominican Republic during the past 100 years [*Lander et al.*, 2002].

2. Size Distribution of Submarine Landslides

[4] We identified 160 landslide scarps within a 12,000 km^2 area of the ocean floor along the northern edge of the tilted carbonate platform north of Puerto Rico and the Virgin Island (Figure 1). The scarps were identified by examining perspective views of the bathymetry from different angles and illuminations, together with slope maps and with seismic reflection profiles, which provide vertical cross-sections of the landslides (Figure 1). Criteria for landslide scarps included a steep headwall and a flat or inverse toe, fissures in the carbonate platform in orientations other than that of the dominant drainage system, and perturbations to the regular stratigraphy of the carbonate layers. Landslide volumes were calculated by interpolating smooth surfaces through polygons that define the edges of each slide, gridding these smooth surfaces, and subtracting these grids from the gridded topography of each scarp (Figure 1c). The grid size for both the topography and the smoothed surface is 50 m.

[5] The volume distribution of 160 slope failures follows a power law, $N_L = 26\ V^{-0.64}$ in the volume range of 0.07–20 km^3 (Figure 2), where N_L, is the cumulative number of failures exceeding a volume, V. The volume distribution of submarine slope failures deviates from a power law for volumes <0.07 km^3 (Figure 2), probably because of undersampling of the many smallest failures, a phenomenon observed in subaerial landslides [*Stark and Hovius*, 2001]. It is therefore, reasonable to assume that hundreds more of small failure scarps exist along the edge of the carbonate platform north of Puerto Rico. However, these hundreds of small slope failures are expected to contribute in total no more than 17 km^3, or 4% of the expected total volume of landslides. In other words, the few largest failure volumes dominate the retreat process of the edge of the carbonate platform. This conclusion is expressed mathematically by a power-law exponent <1.

[6] The two largest observed slope failures have volumes smaller than is predicted by power-law relationship. *Sugai et al.* [1994] noted a similar pattern in landslide distributions

[1]U.S. Geological Survey, Woods Hole Science Center, Woods Hole, Massachusetts, USA.
[2]U.S. Geological Survey, Menlo Park, California, USA.

0094-8276/06/2006GL026125$05.00

in the Akaishi mountains, Japan. It is unclear if physical mechanisms limit landslide volume (a "corner volume") or if the roll-off is caused by under-sampling [*Burroughs and Tebbens*, 2001]. If the roll-off is due to under-sampling, the un-truncated power-law would predict an additional slide with a volume of ~107 km^3, almost 4 times the largest observed failure volume. This volume is significantly smaller than the previously suggested failure of part or the entire amphitheater-shaped scarp north of Arecibo (Figure 1; 1500 km^3 [*Schwab et al.*, 1991]; 900 km^3 [*Mercado et al.*, 2002]), based on lower resolution bathymetry data.

[7] *Dussauge et al.* [2003] found that volume distribution of landslides on subvertical cliffs on land that are classified as rock falls [*Varnes*, 1978] can be fit by a power law with an exponent, b = 0.5 ± 0.2. This distribution is similar to our submarine size distribution, despite its smaller (2–3 orders) volume range. Our submarine slope failures and subaerial landslides also appear similar in their volume-area relationship. This relationship is $V_L = 0.024A_L^{1.368}$ for 201 mapped landslides in the mountains of New Guinea [*Simonett*, 1967], and $V_L = 0.0263A_L^{1.292}$ for our submarine slope failures (Figure 3).

[8] The similarity between the volume distribution of submarine landslides north of Puerto Rico and the distribution of land rock falls may reflect similar underlying physical processes. The landslides are located at the edge of a 1–2 km thick massive and layered limestone [e.g., *van Gestel et al.*, 1999], where slopes exceed 20°. Observations from this area [*ten Brink et al.*, 2006] indicate that slope failures have occurred as rotational slumps, rock slides, and

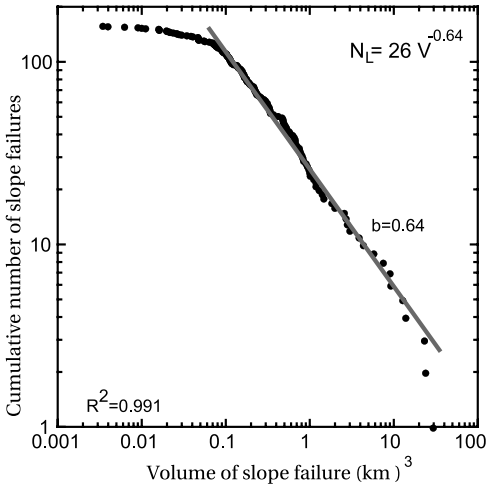

Figure 2. Cumulative volume distribution of submarine slope failures north of Puerto Rico. Dots – observations. Line – best fit regression line on a log-log plot.

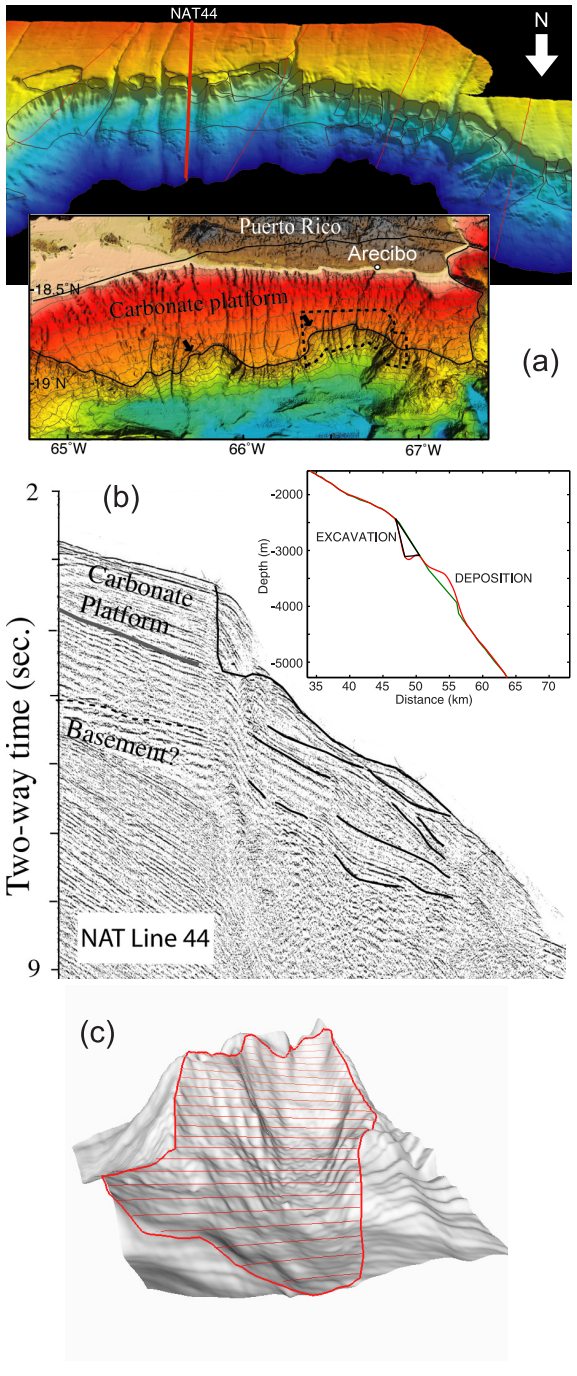

Figure 1. (a) Perspective view of part of the edge of the carbonate platform north of Arecibo, Puerto Rico. View is to the south. Black polygons – interpreted slope failures. Red lines - locations of seismic reflection profiles that aided with the interpretation of landslides. Inset - Bathymetry map of the northern margin of Puerto Rico [*ten Brink et al.*, 2004]. Contour interval is 500 m. Dashed line marks the area of the perspective view. Black lines mark the edges of the tilted carbonate layers. Arrows mark fissures in the carbonate strata. (b) Migrated seismic reflection profile NAT44 showing cross-section of the modeled landslide. Curved reflectors may represent out-of-plane diffractions. Inset - Interpretation of that landslide used as an input to the hydrodynamic model. Green – Pre-failure profile of the slope. Red – Final profile of the slope following excavation of the upper part of the slope and deposition in the lower part. (c) Perspective view of the bathymetry of a single failure scarp (grey shaded) and the smooth surface that was fit within its perimeter (red lines). The failure volume was calculated by subtracting the scarp bathymetry from the depth of the smooth surface.

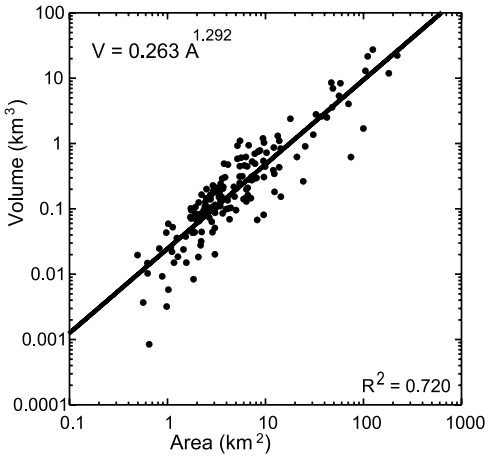

Figure 3. Relationship between volume and area of 156 submarine failure scarps along the edge of the carbonate platform (Figure 1). Four failure areas that are defined by fissures and lack a clear concave shape, were excluded.

debris avalanches (as classified by *Lee et al.* [1993]). *Densmore et al.* [1998] proposed that the probability distribution of subaerial landslide volumes follows a power-law distribution with an exponent that depends on the mechanical properties of the rock mass (cohesion and internal friction angle). Their simulations show rocks with lower cohesion or lower friction coefficient to have b = 1.2, and rocks with higher cohesion or friction coefficient to have b = 0.8. Indeed, subaerial landslides of less consolidated material on lower slopes appear to have a higher exponent (b = 1.2 + −0.3 [*Dussauge et al.*, 2003]).

[9] The similarity between submarine and subaerial landslide distribution may not necessarily extend to other types of slope failures, such as submarine mud flows, turbidity flows, and debris flows (as classified by *Lee et al.* [1993]), because of the role of aqueous overpressure in marine sediments. The 63 mapped clay-rich debris lobes in the Storegga slide [*Haflidason et al.*, 2005], follow almost a linear volume-area relationship ($V_L = 0.0267A_L^{1.032}$, R^2 = 0.708; Figure S1a[1]). This relationship indicates that the thickness of the sliding layer is approximately constant regardless of slide area and is in contrast to the volume/area relationship of Puerto Rico failures, which indicate deeper excavation by larger failures. *Issler et al.* [2005] proposed a logarithmic size distribution for the Storegga debris lobes, not a power law, although their relationship does not account for the largest lobes (100–1300 km^3). However, if we assume undersampling of the smaller lobes (<1 km^3), as in Puerto Rico and in subaerial slides, a power Law, $N_L = 39\ V^{-0.44}$ can be fit for the 31 largest lobes (Figure S1b). The exponent is significantly lower than in Puerto Rico and land rockfalls, probably because of the different failure process.

3. Tsunami Simulation

[10] We next model the tsunami runup expected by the largest failure volume (Figure 1b), located 35 km north of Arecibo, Puerto Rico, whose internal deformation is revealed by a crossing seismic profile (Figure 1b). A simplified representation of this slope failure is parameterized according to its total length (8 km) and is extended laterally to the width of the observed failure (see Table S1). A landslide volume of 22 km^3 is calculated by fitting a smooth surface over the three-dimensional scarp. The landslide is modeled as a region of depletion with a sharp head scarp and a down slope region of deposition, both of nearly equal volumes (Figure 1b) [e.g., *Trifunac et al.*, 2003]. Movement of the landslide is specified according to its duration time (t_d) with smooth ramps used to simulate the accelerating (starting) and decelerating (stopping) phases of slide motion. Slide movement is directly coupled with the hydrodynamic equations of motion through temporal and spatial derivatives of seafloor motion. The hydrodynamic modeling is based on weakly nonlinear "extended" equations [*Lynett and Liu*, 2002]. See auxiliary material for further details.

[11] The maximum tsunami runup on the north coast of Puerto Rico resulting from the largest observed volume failure is estimated at 15.7 m (Figure 4). We systematically vary the failure volume by varying the failure width and keeping the failure profile and the other parameters constant to derive a relationship between tsunami runup and the failure volume (Figure 4, Table S1). For potentially larger slope failures north of Puerto Rico, such as the one estimated from an un-truncated power-law distribution (107 km^3, Figure 2), the maximum predicted runup is 31 m (Figure 4).

[12] We next investigate the smallest failure volume that is capable of generating a damaging tsunami along the north coast of Puerto Rico. There has not been a historical tsunami along this coast, but tsunami runup above 2.5 m along the west coast of Puerto Rico during the 1918 earthquake, resulted in considerable damage and loss of life [*Mercado and McCann*, 1998]. The smallest failure volume that will generate 2.5 m runup on the north coast of Puerto Rico is 5 km^3. Only 9 out of 160 slope failures have a volume ≥5 km^3 (Figure 2). The estimate of the number of devastating tsunamis within the study area is probably

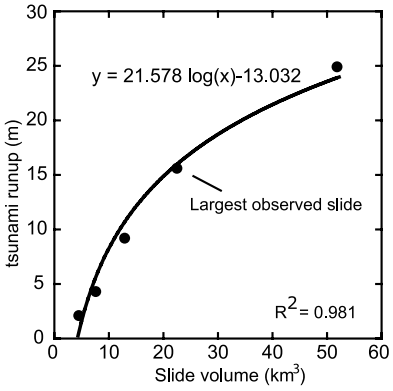

Figure 4. Maximum tsunami runup on the northern coast of Puerto Rico as a function of landslide volume. The runup was calculated for the largest failure volume, shown in Figure 1b, with an observed width of 22 km, volume of 22 km^3, and slide duration of 200 s. Other volumes were calculated by keeping the same landslide profile and varying their width (34, 11, 5.5, and 2.25 km).

[1]Auxiliary material is available at ftp://ftp.agu.org/apend/gl/2006gl026125.

realistic, because the morphology of the coast at Arecibo is typical of the north coast of Puerto Rico, and the modeled failure is closer to the coast than all the other mapped slope failures (Figure 1). A recurrence interval for tsunamis cannot be derived presently because the ages of slope failures north of Puerto Rico are unknown.

[13] The caveat in these predictions is the fact that the calculated runup is highly dependent on the prescribed duration (or velocity) of the landslide (Figure S2). The above runup estimates were calculated using an effective slide velocity of 40 m/s, but the runup will be approximately half as high for a velocity of 20 m/s. (see auxiliary material for further discussion).

4. Conclusions

[14] We have established for the first time the frequency distribution for carbonate submarine slope failures. The volume distribution of submarine slides at edge of the massive carbonate platform north of Puerto Rico follows a power law. This distribution allows estimates of the total volume of slumped material, and indicates that a few largest failures dominate the failure volume. The power law has the same exponent as that for the distribution of subaerial rockfalls despite differences in scale, indicating similar processes. The carbonate slope failure distribution is contrasted with the distribution of the clay-rich Storegga debris flows, which likely reflect different processes.

[15] The submarine failure statistics can be applied to estimates of the impact of landslide-generated tsunami on the north shore of Puerto Rico. The largest mapped slide moving with an assumed slide speed of ~40 m/s could have caused 15.7 m high runup. Only the largest 9 of 160 mapped slope failures could have caused a tsunami runup higher than 2.5 m. Future dating of the failure scarps will allow us to estimate the tsunami recurrence interval north of Puerto Rico.

[16] **Acknowledgment.** We thank VeeAnn Cross for technical assistance, the UTIG Marine Seismic Data Center for seismic lines, and Bill Schwab, David Twichell and Homa Lee, D. Issler, and anonymous for thorough reviews.

References

Burroughs, S. M., and S. F. Tebbens (2001), Upper-truncated power laws in natural systems, *Pure Appl. Geophys.*, *158*, 741–757.

Cornell, C. A. (1968), Engineering seismic risk analysis, *Bull. Seismol. Soc. Am.*, *58*, 1583–1606.

Densmore, A. L., M. A. Ellis, and R. S. Anderson (1998), Landsliding and the evolution of normal-fault-bounded mountains, *J. Geophys. Res.*, *103*, 15,203–15,219.

Dussauge, C., J. Grasso, and A. Helmstetter (2003), Statistical analysis of rockfall volume distributions: Implications for rockfall dynamics, *J. Geophys. Res.*, *108*(B6), 2286, doi:10.1029/2001JB000650.

Fuyii, Y. (1969), Frequency distribution of the landslides caused by heavy rain-fall, *J. Seismol. Soc. Jpn.*, *22*, 244–247.

Haflidason, H., R. Lien, H. P. Sejrup, C. F. Forsberg, and P. Bryn (2005), The dating and morphometry of the Storegga Slide, *Mar. Pet. Geol.*, *22*, 123–136.

Issler, D., F. V. De Blasio, A. Elverhoi, P. Bryn, and R. Lien (2005), Scaling behaviour of clay-rich submarine debris flows, *Mar. Pet. Geol.*, *22*, 187–194.

Lander, J. F., L. S. Whiteside, and P. A. Lockridge (2002), A brief history of tsunamis in the Caribbean Sea, *Sci. Tusnami Hazards*, *20*, 57–94.

Lee, H. J., W. C. Schwab, and J. S. Booth (1993), Submarine landslides: An introduction, in *Submarine Landslides: Selected Studies in the U. S. Exclusive Economic Zone*, edited by W. C. Schwab, H. J. Lee, and D. C. Twichell, U.S. Gov. Print. Off., Washington, D. C.

Lynett, P., and P. L.-F. Liu (2002), A numerical study of submarine landslide generated waves and runup, *Proc. R. Soc. London, Ser. A.*, *458*, 2885–2910.

Malamud, B. D., D. L. Turcotte, F. Guzzetti, and P. Reichenbach (2004), Landslide inventories and their statistical properties, *Earth Surf. Processes Landforms*, *29*, 687–711.

Mercado, A., and W. McCann (1998), Numerical simulation of the 1918 Puerto Rico tsunami, *Nat. Hazards*, *18*, 57–76.

Mercado, A., N. R. Grindlay, P. Lynett, and P. L.-F. Liu (2002), Investigation of the potential tsunami hazard on the north coast of Puerto Rico due to submarine landslides along the Puerto Rico trench, report, 432 pp., Puerto Rico State Emergency Manage. Agency and Sea Grant Coll. Program, San Juan.

Piper, D. J. W., P. Cochonat, and M. L. Morrison (1999), The sequence of events around the epicentre of the 1929 Grand Banks earthquake: Initiation of debris flows and turbidity current inferred from sidescan sonar, *Sedimentology*, *46*, 79–97.

Rundle, J. B., D. L. Turcotte, R. Shcherbakov, W. Klein, and C. Sammis (2003), Statistical physics approach to understanding the multiscale dynamics of earthquake fault systems, *Rev. Geophys.*, *41*(4), 1019, doi:10.1029/2003RG000135.

Satake, K., and Y. Tanioka (2003), The July 1998 Papua New Guinea earthquake: Mechanism and quanitification of unusual tsunami generation, *Pure Appl. Geophys.*, *160*, 2087–2118.

Schwab, W. C., W. W. Danforth, K. M. Scanlon, and D. G. Masson (1991), A giant submarine slope failure on the northern insular slope of Puerto Rico, *Mar. Geol.*, *96*, 237–246.

Simonett, D. S. (1967), Landslide distribution and earthquakes in the Bewani and Torricelli Mountains, New Guinea, in *Landform Studies From Australia and New Guinea*, edited by J. N. Jennings and J. A. Mabbutt, Cambridge Univ. Press, New York.

Stark, C. P., and N. Hovius (2001), The characterization of landslide size distributions, *Geophys. Res. Lett.*, *28*, 1091–1094.

Sugai, T., H. Ohmori, and M. Hirano (1994), Rock control on magnitude-frequency distribution of landslides, *Trans. Jpn. Geomorphol. Union*, *15*, 233–251.

ten Brink, U. (2005), Vertical motions of the Puerto Rico Trench and Puerto Rico and their cause, *J. Geophys. Res.*, *110*, B06404, doi:10.1029/2004JB003459.

ten Brink, U. S., W. W. Danforth, C. Polloni, B. Andrews, P. Llanes, S. V. Smith, E. Parker, and T. Uozumi (2004), New sea floor map of the Puerto Rico trench helps assess earthquake and tsunami hazards, *Eos Trans. AGU*, *85*(37), 349, 354.

ten Brink, U. S., E. L. Geist, P. Lynett, and B. Andrews (2006), Submarine slides north of Puerto Rico and their tsunami potential, in *Caribbean Tsunami Hazard*, edited by A. Mercado, and P. L.-F. Liu, World Sci., Hackensack, N. J.

Trifunac, M. D., A. Hayir, and M. I. Todorovska (2003), A note on tsunami caused by submarine slides and slumps spreading in one dimension with nonuniform displacement amplitudes, *Soil Dyn. Earthquake Eng.*, *23*, 223–234.

van Gestel, J.-P., P. Mann, N. R. Grindlay, and J. F. Dolan (1999), Three-phase tectonic evolution of the northern margin of Puerto Rico as inferred from an integration of seismic reflection, well, and outcrop data, *Mar. Geol.*, *161*, 259–288.

Varnes, D. J. (1978), Slope movements: Types and processes, in *Landslide Analysis and Control*, edited by R. L. Schuster and R. J. Krizek, *Spec. Rep. 176*, pp. 11–33, Transp. Res. Board, Natl. Acad. Sci., Washington, D. C.

Ward, S. N. (2001), Landslide tsunami, *J. Geophys. Res.*, *106*, 11,201–11,215.

B. D. Andrews and U. S. ten Brink, United States Geological Survey, Woods Hole Science Center, 384 Woods Hole Road, Quissett Campus, Woods Hole, MA 02543–1598, USA. (utenbrink@usgs.gov)

E. L. Geist, U.S. Geological Survey, 345 Middlefield Road, MS 999, Menlo Park, CA 94025, USA.